



HAL
open science

Unexpected behavior of InSb alloy for Mg-Ion batteries: unlocking the reversibility of Sb

Lucie Blondeau, Eddy Foy, Hicham Khodja, Magali Gauthier

► To cite this version:

Lucie Blondeau, Eddy Foy, Hicham Khodja, Magali Gauthier. Unexpected behavior of InSb alloy for Mg-Ion batteries: unlocking the reversibility of Sb. *Journal of Physical Chemistry C*, 2018, 123, pp.1120-1126. 10.1021/acs.jpcc.8b10913 . cea-01965738

HAL Id: cea-01965738

<https://cea.hal.science/cea-01965738>

Submitted on 27 Dec 2018

HAL is a multi-disciplinary open access archive for the deposit and dissemination of scientific research documents, whether they are published or not. The documents may come from teaching and research institutions in France or abroad, or from public or private research centers.

L'archive ouverte pluridisciplinaire **HAL**, est destinée au dépôt et à la diffusion de documents scientifiques de niveau recherche, publiés ou non, émanant des établissements d'enseignement et de recherche français ou étrangers, des laboratoires publics ou privés.

Unexpected Behavior of InSb Alloy for Mg-ion Batteries: Unlocking the Reversibility of Sb

Lucie Blondeau,^{1} Eddy Foy,² Hicham Khodja,¹ Magali Gauthier^{1*}*

¹LEEL, NIMBE, CEA, CNRS, Université Paris-Saclay, CEA Saclay, 91191 Gif sur Yvette
Cedex, France

² LAPA-IRAMAT, NIMBE, CEA, CNRS, Université Paris-Saclay, CEA Saclay, 91191 Gif sur
Yvette Cedex, France

*Corresponding authors: magali.gauthier@cea.fr +33 1 69 08 45 30; lucie.blondeau@cea.fr +33

1 69 08 64 96

ABSTRACT

Electrochemical behavior and performance of negative electrodes in metal batteries can be modified and improved by combining different elements. Herein, a beneficial coupling of In and Sb in the alloying reaction with Mg was considered through the preparation of the InSb alloy by mechanochemical synthesis. Despite a strong inactivity of Sb as a sole element in Mg-ion batteries, the combination of Sb with In partially unlocks the reversibility of the alloying reaction of Sb with Mg to form Mg_3Sb_2 . For the first time, this beneficial effect is not only observed during the first magnesiation but along few tens of cycles. The analysis of the behavior of InSb through electrochemical and X-ray diffraction measurements also revealed a more complex path than reported in the literature. Uncommonly a preferential electrochemically-driven amorphization of MgIn is suggested in standard galvanostatic measurements. Crystallization of MgIn is however observed through a galvanostatic intermittent titration technique, suggesting strong kinetic effects on the microstructure, strain or disorder in the InSb phase upon magnesiation.

1. Introduction

The Li-ion batteries production might face some sustainability issues in a near future due to the relatively low abundance and uneven concentration of lithium on the Earth crust and more importantly due to the cobalt criticality. Magnesium (Mg)-based batteries are a promising alternative thanks to Mg high abundance, low price, safety features and its attractive theoretical capacities (2200 mAh g^{-1} and 3800 mAh cm^{-3}).¹⁻⁴ Alike lithium, magnesium metal has a tendency to react with conventional electrolytes. However magnesium transport is limited by the formation of a blocking passivation layer on its surface instead of an ions conducting solid-electrolyte interphase (SEI) for lithium.^{1,2,4-7} This layer impedes the Mg^{2+} ions path to the Mg negative electrode, and thus dramatically limits the reversible stripping/plating electrochemical processes. Aurbach's⁶⁻⁸ group, among others, has overcome this problem in the 2000s, using Grignard reagents in an organohaluminatate-based electrolyte in ethereal solution. Unfortunately, the difficult preparation conditions, their extreme air-sensitive and corrosive characters as well as their instability, limit their use in industry.^{2,4,9,10} Above all, the narrow electrochemical window of organohaluminatate-based electrolytes makes it difficult to develop high-voltage positive electrode materials.^{6,8} An interesting alternative for the development of magnesium batteries is to replace magnesium metal with a negative electrode material, which should be compatible with conventional electrolytes. Such Mg-ion cells could be a reliable alternative to lithium-based systems. Recently, some studies showed that *p*-block elements (Sn,¹¹⁻¹⁷ Sb,^{18,19} In,^{17,20,21} Pb,²² Bi,^{5,18,23-27}...) can electrochemically alloy with Mg and can be stable with conventional electrolyte such as $\text{Mg}(\text{TFSI})_2$ dissolved in a glyme solvent.^{5,26} Despite their interesting electrochemical reactivity, these alloys present lower theoretical gravimetric capacities than Mg metal (300 to 900 mAh g^{-1})¹¹⁻²¹. However, their theoretical volumetric capacity can compete with Li or Mg metal, with for example a value of $\sim 1900 \text{ mAh cm}^{-3}$ for bismuth. Among these

elements, indium presents the lowest alloying potential ($0.09V_{Mg}$) and a good reversibility but suffers from kinetics limitations at high rates and scarce resources.^{17,20} Differently, antimony presents one of the highest theoretical capacity ($660mAh\ g^{-1}$),^{18,19} despite its lack of electrochemical activity as pure element. Magnesiumation of pure Sb to form Mg_3Sb_2 was only observed in thin films,¹⁹ while poor– if any– alloying occurs for pure micrometric Sb particles.¹⁸ In any case, Sb electrodes present a strong irreversibility and capacity fading.^{18,19}

$Bi_{1-x}Sb_x$ and SnSb alloys were respectively investigated by Murgia et al.¹⁸ and Parent et al.¹¹ as negative electrodes for Mg-ion batteries to seek for a synergy between the different elements. The first authors evidenced that antimony can be activated when coupled with bismuth. However, this beneficial effect is only observed on the first magnesiumation as Mg^{2+} ions cannot be pulled out of the Mg_3Sb_2 structure in the subsequent demagnesiumation.¹⁸ Differently, Parent et al.¹¹ revealed that the electrochemical reaction with Mg modifies SnSb particles into a network of Sn and Sb subparticles, where only Sn remains electroactive. The presence of Sb, inactive towards Mg, enhances the performance of Sn through the formation of an interface stabilizing Sn into its cubic phase. A beneficial coupling of In and Bi in the InBi alloy was also explored by Murgia et al.²¹ No clear synergy exists in InBi but a complex conversion-type electrochemical mechanism with multiple intermediate phases was evidenced.²¹

In this work, a synergy between In and Sb in the InSb alloy was investigated by electrochemical analysis and *ex situ* X-Ray Diffraction (XRD). In a new way, Sb is shown to reversibly react in part with Mg. An electrochemically-driven amorphization²⁸ is here demonstrated for the first time for MgIn in Mg-ion batteries, by analogy with other alloys such as silicon in Li-ion batteries²⁸ or SnSb in Na-ion batteries.²⁹

2. Methods

In (Alpha Aesar, 99.99%) and Sb (Alpha Aesar, 99.5%) powders were purchased and used as received. The InSb compound was prepared by planetary ball milling in a Fritsch Pulverisette with 3 stainless steel balls in a stainless-steel vial. In and Sb powders were introduced in stoichiometric amount with a ball-to-powder ratio of 1:70 and milled for 6 h under inert atmosphere (Ar). A milling yield (corresponding to the ratio of powder masses after and before milling) higher than 95% was obtained, demonstrating poor welding between the powder and the balls/vial.

Powders samples were characterized by XRD on a RU-200B rotating anode X-ray generator using monochromotized Mo radiation ($\lambda=0.7093\text{\AA}$). Scanning Electron Microscopy (SEM) was performed on a SEM-FEG Zeiss Ultra 55 model operating at 3kV in order to study the morphology of the InSb powder.

Composite electrodes were formulated by mixing 80 wt.% of the InSb ball-milled active material with 10 wt.% of carbon (Csp, 99+ %, Alfa Aesar) and 10 wt.% of polyvinylidene fluoride (PVDF, Solvay Solef) with N-methyl-2-pyrrolidone (NMP, 99 %, Acros Organics) as the solvent. The slurry was stirred for 30 min before being cast onto a Cu foil (99.8%, Alfa Aesar). The film was dried at room temperature during 24 h and subsequently for 24 h at 120°C under vacuum. Electrode disks were cut out and stored in a glove box. The average active material loading was around 0.35 – 0.52 mg.cm⁻².

Electrochemical tests were performed in a half-cell configuration using 2-electrodes Swagelok-type cells with a Mg disc (99.95%, Gallium Source) as both reference and negative electrode. Whatman GF/A glass microfiber filters were used as separators. The electrolyte consists of a mixture of ethylmagnesium chloride (EtMgCl, 2.0 M in THF, Sigma-Aldrich) and

diethylaluminium chloride (Et_2AlCl , 97 %, Sigma-Aldrich) in a 1:1 molar ratio solubilized in anhydrous tetrahydrofuran (THF, 99.9 %, Carlo-Erba). The final concentration of the organohaluminat complex “ $\text{EtMgCl-Et}_2\text{AlCl}$ ” is estimated $\sim 0.35 \text{ mol. L}^{-1}$. All the operations of cell assembly were made in an Ar-filled glove box. Galvanostatic tests were performed at room temperature using a research-grade potentiostat (VMP3, Biologic) between 0.005 and 0.8 V_{Mg} (vs. Mg^{2+}/Mg). The electrochemical tests were performed at $C/50$, if not otherwise mentioned, where C/n rate means that the full magnesiation is reached in n hours. $C/50$ rate corresponds here to a current density of 11 mA g^{-1} . A galvanostatic intermittent titrate technique (GITT), which consists of a series of current pulses (CCV : constant current voltage), each followed by a relaxation time (OCV : open-circuit voltage), was used to study the electrochemical mechanisms. In our case pulse periods of 1 h at a $C/50$ rate followed by open circuit current (OCV) periods for 2 h were used. Every electrochemical test was repeated at least three times to verify the reproducibility.

Ex situ XRD characterization after cycling was performed on electrodes previously washed with THF to avoid any trace of the electrolyte. To avoid reactivity with air, all XRD measurements were carried out by protecting the sample with Kapton tape in the glove box.

3. Results and discussion

High energy mechanochemical synthesis is known as an efficient method to synthesize intermetallic compounds^{18,21,30–32} such as InSb.³³ The XRD pattern (Figure 1) and the profile matching (Supplementary Information, Figure S1) collected on the synthesized powder shows the formation of a cubic phase corresponding to the InSb compound with crystallographic parameters in agreement with the literature (space group $F\bar{4}3m$, $a = 6.476 \text{ \AA} \pm 0.003^{34}$). A small

diffraction reflex at 18° is also detected and is explained by iron impurities from the vial and balls during the milling process. The SEM image (Figure 1b) evidences the formation of large micrometric aggregates of around 1 to 10 μm made of sub-micrometric particles roughly welded together.

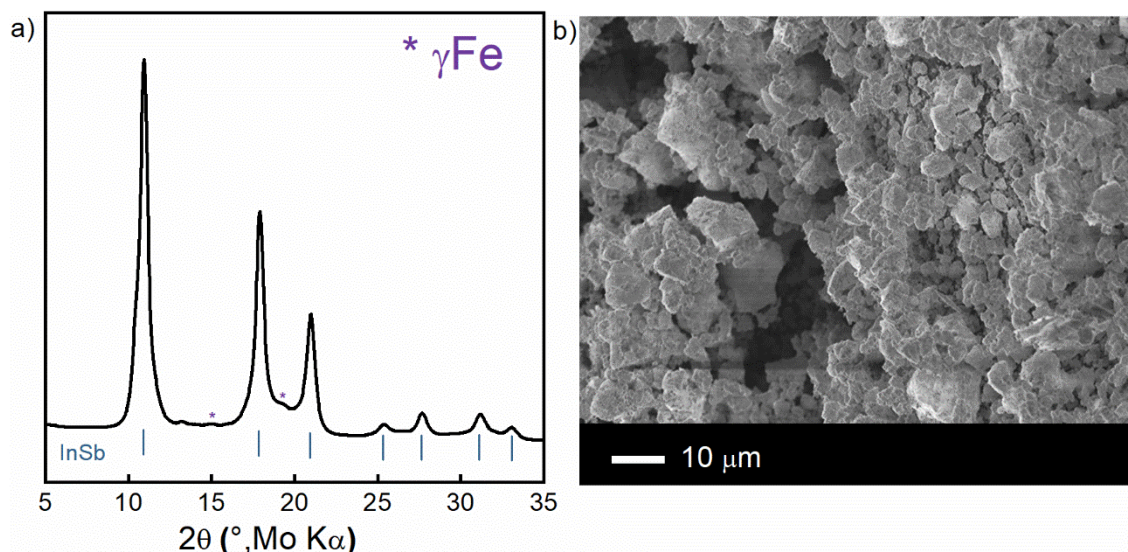


Figure 1. (a) XRD pattern and (b) SEM picture of the InSb powder obtained by high energy ball-milling (Bragg position of InSb as blue vertical bars).

3.1. Electrochemical mechanism of InSb-Mg alloying: competition between crystallization and electrochemically-driven amorphization

To determine if a beneficial coupling between In and Sb exists, the electrochemical properties of the InSb alloy were first compared with the behaviour of a simple mixture of pure micrometric In and Sb powders in stoichiometric amounts. The first magnesiation of the In+Sb blend (Supplementary Information, Figure S2) presents only one electrochemical plateau at $\sim 0.09 V_{\text{Mg}}$ and only 0.6 Mg^{2+} are inserted in the electrode. The voltage value of the plateau is characteristic of the reactivity of In with Mg.²⁰ Therefore, only In is reacting while Sb is completely inactive.

This is expected as no electrochemical activity for Sb micrometric particles was observed previously with a fast decrease of potential down to $0V_{Mg}$.^{18,19} On the contrary, the InSb composite electrode (Figure 2a) is able to host 1.9 moles of Mg^{2+} in its structure, demonstrating a beneficial effect between the two elements. The electrochemical profile suggests that Sb is electrochemically activated by the presence of In. This behavior seems comparable to what was already showed by Murgia et al.¹⁸ for the $Bi_{1-x}Sb_x$ where antimony is activated in the presence of Bi for the first magnesiation, and will be discussed in more details below.

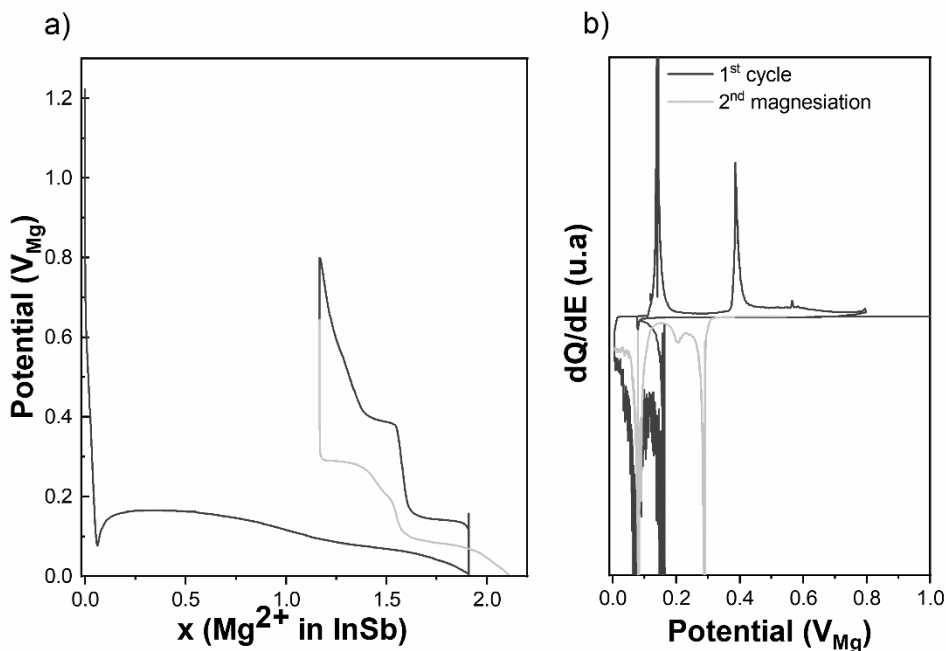
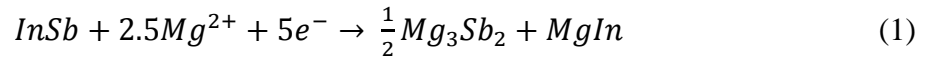


Figure 2. (a) Galvanostatic cycling of an InSb/Mg battery at a $C/50$ rate and (b) corresponding incremental capacity profile.

The first 1.5 cycle of the InSb/Mg battery at a constant rate of $C/50$ in galvanostatic mode (GCPL) and the corresponding incremental capacity (Figure 2a, b) shows a drastic change between the first and the second cycle. The first magnesiation exhibits two principal regions

barely separated (Figure 2a). However, the presence of two electrochemical reactions appears more clearly on the representation of the incremental capacity (Figure 2b), where two peaks at approximately 0.16 V_{Mg} and 0.07 V_{Mg} can be noted. As already reported in the literature, pure In electrodes display a flat plateau around 0.09 V_{Mg} related to the two-phase reaction leading the formation of crystalline MgIn (Figure S3).²⁰ For the Sb electrodes, the two-phase reaction with Mg is predicted at 0.31 V_{Mg} to form Mg_3Sb_2 .^{18,19} Therefore, the alloying region around 0.16 V_{Mg} (before ~ 1.25), should be linked to the formation of Mg_3Sb_2 . The second region occurring at a lower potential around 0.07 V_{Mg} should be associated with the reaction of In with Mg to form MgIn. This agrees well with the electrochemical reactivity of the pure In and Sb elements,^{19,20} and can be summarized as follows:



At the beginning of the first magnesiation, the cell voltage drops rapidly down to $\sim 0.07 V_{Mg}$ (this value varies between 0.05-0.1 V_{Mg} depending on the cell) but then rises again to finally reach the first alloying plateau at 0.16 V_{Mg} . As already seen in other materials^{5,13,19,22,24} this can be related to the equilibrium between first the nucleation of the Mg_3Sb_2 grains and second the growth of the particles. The Mg-In/Sb electrochemical alloying potentials are not really stable in the first magnesiation but, at the end, the system reaches a capacity of 535 mAh g^{-1} which is very close to the theoretical capacity of 566 mAh g^{-1} (calculated based on the formation of Mg_3Sb_2 and MgIn).

The first demagnesiation (Figure 2a, b) shows two well-defined plateaus at 0.39 V_{Mg} and 0.14 V_{Mg} . Considering the dealloying potential values of Mg_3Sb_2 ^{18,19} and MgIn,^{20,21} the higher plateau is attributed to the dealloying of Mg_3Sb_2 , while the second is assigned to MgIn dealloying. Mg dealloying reaction occurs at 0.14 and 0.39 V_{Mg} during charge so the system presents a

consequential polarization of about 230 mV (for the alloy Mg_3Sb_2) and 80 mV (for MgIn). The system is poorly reversible at the first cycle, with a capacity retention of only 39 % (Figure 2a). Few factors can explain this low reversibility. The large volume expansion during the first cycle (theoretical volume expansion estimated $\sim 100\%$) could lead to the disconnection of some active material particles from the global matrix, or Mg^{2+} diffusion can be impeded in some large particles due to the sluggish diffusion of Mg^{2+} in solids.⁵⁻⁹ A reactivity between the electrode and the electrolyte could also irreversibly consume electrons and/or Mg^{2+} ions, implying a poor stability of the alloy in the electrolyte, in contradiction to the expected stability of THF based solutions.³⁵ Most probably, we believe that the irreversibility could arise from the poor ability of the Mg_3Sb_2 to be demagnesiased.^{18,19}

In contrast with the first cycle, the second magnesiased (Figure 2a, b) exhibits two clear plateaus around 0.3 and 0.08 V_{Mg} in agreement with the reactivity of Sb ^{18,19} and In ²⁰ and a small third flexion in between at 0.21 V_{Mg} . The small third flexion may highlight a change in the electrochemical pathway, with for example a reorganization of the material structure upon alloying, or an electrochemical reactivity of some impurities in the powder. The presence of the higher plateau at 0.3 V_{Mg} demonstrates that Sb is not only active at the first cycle but can partially be reversible upon cycling. This confirms the peculiar beneficial effect provided by the presence of In with Sb . Strong morphology modification in the active material²¹ upon the first cycle could explain the large profile difference observed between the first and the second magnesiased. In fact, the electrochemical reaction can induce a complete disaggregation of the initial micrometric grains of active materials, inducing a grinding of the material explaining the different electrochemical behavior between the first and second cycle.²¹

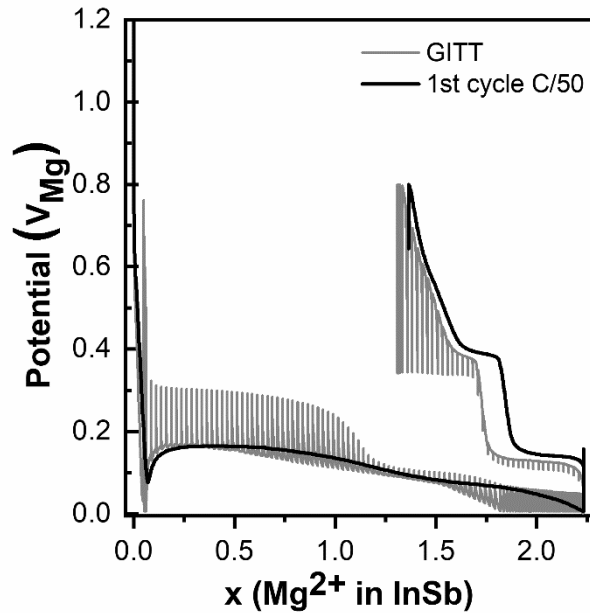


Figure 3. GITT profile (grey) at the first cycle obtained from an InSb/Mg battery (1 h of reduction/oxidation at a C/50 rate followed by 2 hours of relaxation) compared with the galvanostatic cycling at a C/50 rate (black).

In order to better understand the mechanism of Mg alloying/de-alloying in InSb, a galvanostatic intermittent titration technique (GITT) was applied (Figure 3) and compared with the conventional galvanostatic cycling described previously (Figure 2a). The procedure allows the electrode to reach its equilibrium potential and can provide insights on the kinetics phenomena. Following the OCV points on the GITT, it is possible to see a different behavior upon alloying than the GCPL and a similar trend during the dealloying. In contrast to the conventional cycling, the thermodynamic potentials of alloying processes are clearly defined with two plateaus upon the magnesianation in GITT (Figure 3). The plateaus of the first magnesianation are observed around 0.3 and 0.06 V_{Mg} compared to 0.16 and 0.07 V_{Mg} for the GCPL. The successive formations of Mg_3Sb_2 and $MgIn$ upon magnesianation of InSb are further confirmed. The polarization is reduced to 40 mV for both Mg_3Sb_2 and $MgIn$ compared to 230

mV_{Mg} and $80 mV_{Mg}$ in the conventional galvanostatic test respectively. The large difference observed between CCV and OCV value in the Mg_3Sb_2 formation region reveals a kinetic limitation at the first cycle, which will be discussed later on.

The conclusions drawn above on the formation of Mg_3Sb_2 and $MgIn$ as products of the alloying reactions of InSb with Mg were confronted with *ex situ* XRD measurements on InSb composite electrodes cycled at C/100 rate. To follow the formation of the Mg alloys and to better understand the reaction mechanisms, cells were stopped and electrodes removed at different states of the magnesiation. The corresponding XRD patterns are presented on Figure 4 (complete patterns on Figure S4).

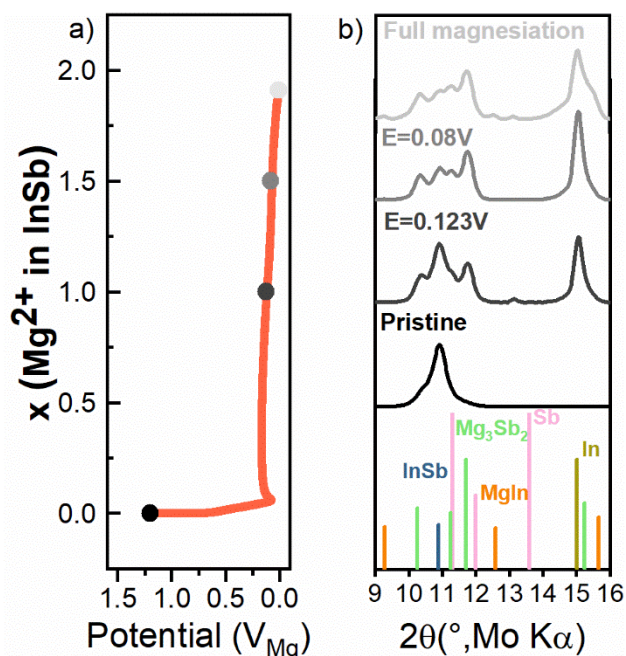


Figure 4. *Ex situ* XRD patterns collected on InSb-based composite electrodes stopped at different states of the magnesiation at a C/50 rate. The vertical bars show the Bragg position of InSb (blue), MgIn (orange), In (brown), Sb (pink) and Mg_3Sb_2 (green).

The phase evolutions on the first magnesiation are discussed in the following points:

At the beginning of the magnesiation, up to the reaction of $\sim 1 \text{ Mg}^{2+}$, a large decrease of the InSb reflex and an increase of new reflexes at 10.3° , 11.2° and 11.7° are observed. These new reflexes are characteristic of Mg_3Sb_2 ³⁶ and therefore confirms the magnesiation of Sb to form Mg_3Sb_2 , in agreement with the electrochemical data. Simultaneously another diffraction reflex corresponding to pure metallic indium³⁷ appears at 15.0° , indicating that In is extruded from the InSb alloy, as already seen in the lithiation of InSb.³⁸

After the alloying of around 1.5 Mg^{2+} within the material, Mg_3Sb_2 and pure In are still detected, while the intensity of the characteristic reflex of InSb at 10.9° decreases.

After full magnesiation, Mg_3Sb_2 and pure In are still observed while some InSb remains, revealing that not all the active material has reacted. Surprisingly, while the electrochemical profile and ex situ diffraction data of In electrodes will suggest the formation of crystalline MgIn (Figure S3), only a small contribution of crystalline MgIn is supposedly detected with the small reflexes appearing at 9.3° , 12.8° and 15.6° ($P4/mmm \text{ MgIn}$)³⁹. It is worth mentioning that the diffraction reflex of Mg_3Sb_2 at 15.2° is close to the main reflex at 15.6° of MgIn, rendering the analysis of the patterns relatively complex. Above all, it is important to note that the characteristic reflexes of MgIn were not always observed on fully magnesiated samples when the tests were reproduced (Figure S5), suggesting the presence of MgIn in an amorphous state.

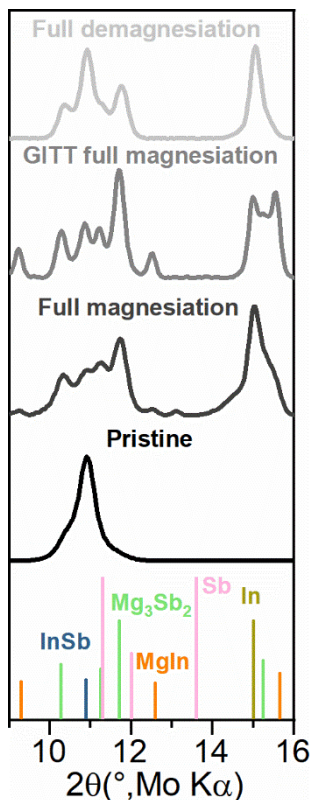


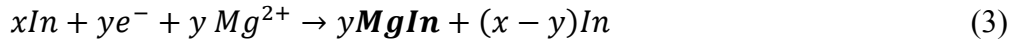
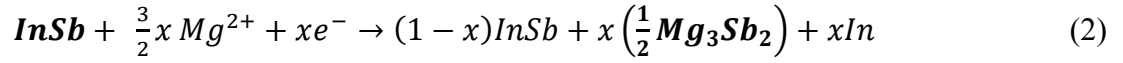
Figure 5. *Ex situ* XRD patterns collected on the pristine InSb powder, and on electrodes stopped at the end of the magnesiatio at a C/100 rate either with a galvanostatic cycling or in GITT mode, and on an electrode cycled at a C/100 rate and stopped at the end of the first cycle (demagnesiatio). The vertical bars show the Bragg position of InSb (blue), MgIn (orange), In (brown), Sb (pink) and Mg₃Sb₂ (green).

To better identify the phases present during Mg alloying in InSb, XRD patterns from samples fully magnesiatio either at a C/100 rate or in GITT mode were compared (Figure 5, complete patterns on Figure S6). The XRD pattern of the GITT sample collected at the end of the first magnesiatio shows a different profile in comparison with the GCPL sample pattern. Interestingly the XRD pattern of the GITT magnesiatio sample presents sharper and better-

defined reflexes, denoting more highly-crystallized phases. More importantly, the main difference is the unambiguous presence of three sharp reflexes at 9.3° , 12.8° and 15.6° which corresponds to the P4/mmm MgIn phase. MgIn crystallization is clearly evidenced on the GITT sample –in which the electrode is allowed to reach a steady state– while the crystallization is circumvented with the GCPL sample. The presence of amorphous MgIn seems counterintuitive as the magnesiation of pure In²⁰ (Figure S3) and of an InBi alloy²¹ leads to crystalline MgIn. However the capacity extracted from InSb (Figure 2) can not only be justified by the alloying/dealloying process of Sb. The relatively small proportion of crystalline MgIn, if any, observed in the GCPL electrode, compared to what is expected from the electrochemical profile and capacity recovered, indirectly suggests an electrochemically-driven amorphization of the MgIn phase. The crystallization of MgIn is thus kinetically dependent, implying a struggle between amorphization and crystallization depending on the rate applied. What frustrates the crystallization of MgIn has still to be fully rationalized. However, we can suggest that the extrusion of In from InSb during the first part of the magnesiation could cause dramatic changes of morphology and/or enhance the atomic disorder and create nanosized domains of In (electrochemical grinding). The formation of highly reactive In nanoparticles could completely modify the reaction path of In with Mg and conducts to the formation of a nanosized amorphous MgIn phase. Moreover, the sluggish diffusion of Mg²⁺ could slow down the atomic rearrangement in the MgIn structure, while an inner strain could also hinder the formation of crystalline MgIn.²⁹ In order to confirm our hypotheses, some *in situ* XRD and *in situ* X-ray absorption experiments should be performed to identify the phases formed at a more local scale.

By coupling the XRD characterization and electrochemical data, we thus propose the following reaction pathway for the first magnesiation of InSb, based on two successive biphasic

reactions governed by the magnesiation of Sb and In, with first an extrusion of In and then an incomplete transformation of the InSb material which leads to the crystallization of Mg₃Sb₂ and the electrochemically-driven amorphization of MgIn using galvanostatic cycling:



Finally, we also investigated the phases formed at the end of the first cycle. The XRD pattern acquired on a completely demagnesiated electrode is shown in Figure 5. Interestingly, the first demagnesiation does not produce Sb and In as pure elements from the demagnesiation of MgIn and Mg₃Sb₂ phases, but instead the intermetallic compound InSb is reformed as the major product. Nevertheless, some Mg₃Sb₂ and In still remain which demonstrates an uncompleted demagnesiation of the overall electrode and explain for the most part the large irreversibility observed in the first cycle.

3.2. Cycling performance and evidence for Sb electrochemical activation

The study of InSb-based composite electrodes was firstly proposed to investigate a possible synergy between In and Sb. The alloy could present a better capacity due to the high capacity of the antimony, namely 660 mAh g⁻¹,^{18,19} and the lowest working potential of indium among the other p-block elements.^{20,21} It is interesting, from a fundamental point of view, to evaluate the electrochemical performance and to compare them with In and Sb-based electrodes already reported in the literature.^{18,20}

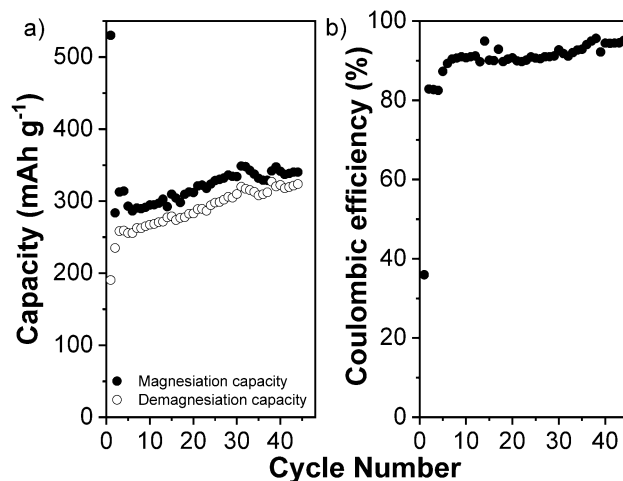


Figure 6. (a) Evolution of the capacity of magnesianation and demagnesianation of InSb/Mg battery at a C/50 rate during 50 cycles and (b) of the corresponding coulombic efficiency.

Electrochemical cycling tests at a C/50 rate were performed upon more than 40 cycles on an InSb-based electrode (Figure 6). Despite the lack of activity of the pure Sb reported previously, the InSb alloy presents capacities higher than indium composite electrodes (first magnesianation capacity around 460 mAh g⁻¹ (theoretical capacity 467 mAh g⁻¹)²⁰ at least for the first cycle. After the first cycle a sharp decrease of the capacity is observed and then the capacity stabilizes for both alloying and dealloying reactions with a slight gradual increase from 270 to 350 mAh g⁻¹. The capacity recovery upon cycling can be related to an *in situ* nanostructuration of the active material during cycling allowing a deeper diffusion of Mg²⁺ ions into the electrode and therefore generating a more important proportion of InSb being active towards Mg²⁺. However, electrolyte's degradation along cycling can also possibly explain the extra-capacity observed and give the impression of a global increase of the capacity. These capacities observed are nevertheless lower than those reached with pure In electrodes. Murgia et al.²⁰ showed a first

magnesium capacity of 460 mAh g⁻¹ with then capacities stabilizing approximately around 440 mAh g⁻¹. Nevertheless, we evidence for the first time a partial reversibility of Sb in an electrode for Mg-ion batteries. The proportion of the magnesium capacity due to Mg₃Sb₂ was calculated based on the capacity obtained on the first alloying plateau (Figure 7). The formation of Mg₃Sb₂ is responsible for ~ 42% of the capacity at the first magnesianation while the value then slowly decreases to reach ~ 20% after 20 cycles and ~ 10% after 40 cycles. This confirms that Sb is electrochemically activated by the presence of In and that its contribution to the total capacity is not negligible. Despite a large irreversible capacity at the first cycle, we show that InSb cycling promotes the reactivity of Sb, not only at the first magnesianation, but also upon further cycling. The activation of Sb in InSb could be explained by the formation of a peculiar interface favoring Sb reactivity. This has already been observed in the promotion of Sn reactivity in SnSb by the presence of Sb, despite the inactivity of Sb in the material.^{11,12} Finally, we also suggest a possible effect of a different microstructure in the InSb material compared to a pure micrometric Sb powder. The different microstructure inside the active material could stimulate the reactivity of Sb and create a highly reactive Mg₃Sb₂ phase more prone to demagnesianation. These hypotheses need to be confirmed with further investigations.

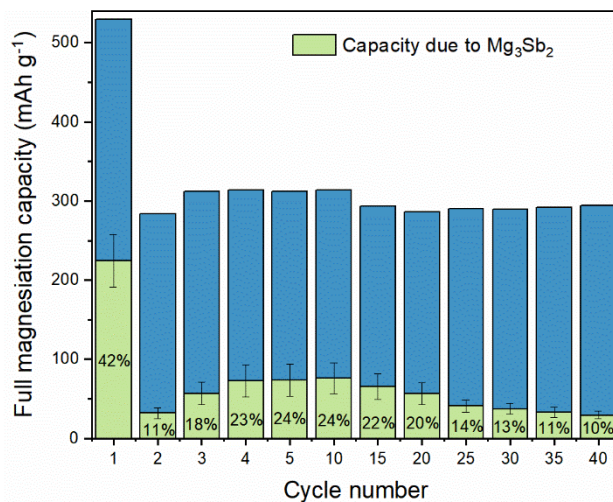


Figure 7. Evolution of the full capacity of magnesian of InSb/Mg battery and of the part of the capacity corresponding to the contribution of Mg₃Sb₂ (green) at a C/50 rate during 40 cycles.

The electrochemical performance of the micrometric InSb-based electrode was also evaluated through rate capability test from C/50 to 1C (Figure S7). It shows a steady decrease of the capacity with the increase of the current density. The capacity is maintained above 200 mAh g⁻¹ until a C/25 rate while it then regularly decreases to reach almost no capacity at 1C. These results manifest kinetics limitations during the InSb magnesian/demagnesian processes. This emphasizes the sluggish diffusion of Mg²⁺ in the solid and is probably accentuated by the reactivity of antimony^{18,19} in the alloy and the high stability of the ionic Mg-Sb bonds⁴⁰ in the Mg₃Sb₂ phase. However, we want to stress out that the present study was first aimed at understanding the fundamental electrochemical behavior of InSb, thus formulations of the electrode and the electrolyte have not been optimized. We believe that nanostructuring of the material could improve this performance by reducing the diffusion paths for Mg²⁺ ions.

4. Conclusion

The electrochemical reactivity and performance of the InSb alloy as a negative electrode for Mg-ion batteries have been investigated. As expected from the literature on pure In and Sb, the potential profile of the first magnesiation evidences two successive two-phase reactions corresponding to the formation of Mg_3Sb_2 and MgIn . However, surprisingly, XRD patterns collected at different magnesiation states suggest a kinetically dependent electrochemically-driven amorphization of MgIn . This phenomenon seems unique to the InSb phase as crystalline MgIn has always been detected in the literature in the case of pure In or InBi electrodes. This behavior suggests a possible competition between crystallization and amorphization in the material which could be explained by an increase of disorder at the atomic scale in the material, an internal strain or modification of the microstructure upon reaction. Further studies are required to understand the driving force the amorphization of MgIn , and how it can influence the electrochemical behavior and performance of InSb, and in a broader context of alloy materials in metal batteries. Additionally, we also revealed a strong synergy between In and Sb in InSb, with the promotion of the electrochemical activity of Sb towards magnesiation. In contrast to what was already reported in other studies, Sb is shown for the first time to be able to partially react reversibly with Mg along few cycles. The first magnesiation reaches a capacity $> 500 \text{ mAh g}^{-1}$ and some subsequent capacities around 300 mAh g^{-1} . Some questions remain on the mechanisms leading to the activation of Sb in the InSb alloy, whether it can involve a peculiar interface in the material or be related to the microstructure. This requires further investigation for example with *in situ* XRD/X-ray absorption to understand how to further trigger the full reactivity of Sb in Mg-ion batteries.

Supporting Information

Supplementary electrochemical data and *ex situ* X-Ray Diffraction data

Conflicts of interest

There are no conflicts to declare.

Acknowledgment

Financial funding from the Agence Nationale de la Recherche (ANR) of France under the contract ANR-16-CE05-0004 is acknowledged.

References

- (1) Song, J.; Sahadeo, E.; Noked, M.; Lee, S. B. Mapping the Challenges of Magnesium Battery. *J. Phys. Chem. Lett.* **2016**, *7*, 1736–1749.
- (2) Yoo, H. D.; Shterenberg, I.; Gofer, Y.; Gershinshy, G.; Pour, N.; Aurbach, D. Mg Rechargeable Batteries: An on-Going Challenge. *Energy Environ. Sci.* **2013**, *6*, 2265–2279.
- (3) Muldoon, J.; Bucur, C. B.; Gregory, T. Quest for Nonaqueous Multivalent Secondary Batteries: Magnesium and Beyond, *Chem. Rev.*, **2014**, *114*, 11683–11720.
- (4) Bucur, C. B.; Gregory, T.; Oliver, A. G.; Muldoon, J. Confession of a Magnesium Battery, *J. Phys. Chem. Lett.*, **2015**, *6*, 3578–3591.
- (5) Shao, Y.; Gu, M.; Li, X.; Nie, Z.; Zuo, P.; Li, G.; Liu, T.; Xiao, J.; Cheng, Y.; Wang, C.; et al. Highly Reversible Mg Insertion in Nanostructured Bi for Mg Ion Batteries. *Nano Lett.* **2014**, *14*, 255–260.

- (6) Aurbach, D.; Schechter, A.; Moshkovich, M.; Cohen, Y. On the Mechanisms of Reversible Magnesium Deposition Processes. *J. Electrochem. Soc.* **2001**, *148*, A1004–A1014.
- (7) Mizrahi, O.; Amir, N.; Pollak, E.; Chusid, O.; Marks, V.; Gottlieb, H.; Larush, L.; Zinigrad, E.; Aurbach, D. Electrolyte Solutions with a Wide Electrochemical Window for Rechargeable Magnesium Batteries. *J. Electrochem. Soc.* **2008**, *155*, A103–A109.
- (8) Aurbach, D.; Gizbar, H.; Schechter, A.; Chusid, O.; Gottlieb, H. E.; Gofer, Y.; Goldberg, I. Electrolyte Solutions for Rechargeable Magnesium Batteries Based on Organomagnesium Chloroaluminate Complexes. *J. Electrochem. Soc.* **2002**, *149*, A115–A121.
- (9) Mohtadi, R.; Mizuno, F. Magnesium Batteries: Current State of the Art, Issues and Future Perspectives. *Beilstein J. Nanotechnol.* **2014**, *5*, 1291–1311.
- (10) Aurbach, D.; Lu, Z.; Schechter, A.; Gofer, Y.; Gizbar, H.; Turgeman, R.; Cohen, Y.; Moshkovich, M.; Levi, E. Prototype Systems for Rechargeable Magnesium Batteries. *Nature* **2000**, *407*, 724.
- (11) Parent, L. R.; Cheng, Y.; Sushko, P. V.; Shao, Y.; Liu, J.; Wang, C.-M.; Browning, N. D. Realizing the Full Potential of Insertion Anodes for Mg-Ion Batteries Through the Nanostructuring of Sn. *Nano Lett.* **2015**, *15*, 1177–1182.
- (12) Cheng, Y.; Shao, Y.; Parent, L. R.; Sushko, M. L.; Li, G.; Sushko, P. V.; Browning, N. D.; Wang, C.; Liu, J. Interface Promoted Reversible Mg Insertion in Nanostructured Tin–Antimony Alloys. *Adv. Mater.* **2015**, *27*, 6598–6605.
- (13) Singh, N.; Arthur, T. S.; Ling, C.; Matsui, M.; Mizuno, F. A High Energy-Density Tin Anode for Rechargeable Magnesium-Ion Batteries. *Chem. Commun.* **2012**, *49*, 149–151.

- (14) Singh, N.; Matsui, M. Bismuth-Tin Binary Anodes for Rechargeable Magnesium-Ion Batteries, US Patent 8647770 B2, February 11, 2014.
- (15) Kitada, A.; Kang, Y.; Uchimoto, Y.; Murase, K. Electrochemical Reactivity of Magnesium Ions with Sn-Based Binary Alloys (Cu-Sn, Pb-Sn, and In-Sn). *ECS Trans.* **2014**, *58*, 75–80.
- (16) Yaghoobnejad Asl, H.; Fu, J.; Kumar, H.; Welborn, S. S.; Shenoy, V. B.; Detsi, E. In Situ Dealloying of Bulk Mg₂Sn in Mg-Ion Half Cell as an Effective Route to Nanostructured Sn for High Performance Mg-Ion Battery Anodes. *Chem. Mater.* **2018**, *30*, 1815–1824.
- (17) Singh, N.; Matsui, M. Indium-Tin Binary Anodes for Rechargeable Magnesium-Ion Batteries, US Patent 8673493 B2, March 18, 2014.
- (18) Murgia, F.; Laurencin, D.; Weldekidan, E. T.; Stievano, L.; Monconduit, L.; Doublet, M.-L.; Berthelot, R. Electrochemical Mg Alloying Properties along the Sb_{1-x}Bi_x Solid Solution. *Electrochim. Acta* **2018**, *259*, 276–283.
- (19) Arthur, T. S.; Singh, N.; Matsui, M. Electrodeposited Bi, Sb and Bi_{1-x}Sb_x Alloys as Anodes for Mg-Ion Batteries. *Electrochem. Commun.* **2012**, *16*, 103–106.
- (20) Murgia, F.; Weldekidan, E. T.; Stievano, L.; Monconduit, L.; Berthelot, R. First Investigation of Indium-Based Electrode in Mg Battery. *Electrochem. Commun.* **2015**, *60*, 56–59.
- (21) Murgia, F.; Monconduit, L.; Stievano, L.; Berthelot, R. Electrochemical Magnesiumation of the Intermetallic InBi through Conversion-Alloying Mechanism. *Electrochim. Acta* **2016**, *209*, 730–736.

(22) Periyapperuma, K.; Tran, T. T.; Purcell, M. I.; Obrovac, M. N. The Reversible Magnesiumation of Pb. *Electrochim. Acta* **2015**, *165*, 162–165.

(23) Ramanathan, M.; Benmayza, A.; Prakash, J.; Singh, N.; Mizuno, F. A Porous Electrode Model for the Magnesiumation and Demagnesiumation of a Bismuth Electrode in Rechargeable Magnesium-Ion Cells. *J. Electrochem. Soc.* **2016**, *163*, A477–A487.

(24) DiLeo, R. A.; Zhang, Q.; Marschilok, A. C.; Takeuchi, K. J.; Takeuchi, E. S. Composite Anodes for Secondary Magnesium Ion Batteries Prepared via Electrodeposition of Nanostructured Bismuth on Carbon Nanotube Substrates. *ECS Electrochem. Lett.* **2015**, *4*, A10–A14.

(25) Wang, W.; Liu, L.; Wang, P.-F.; Zuo, T.-T.; Yin, Y.-X.; Wu, N.; Zhou, J.-M.; Wei, Y.; Guo, Y.-G. A Novel Bismuth-Based Anode Material with a Stable Alloying Process by the Space Confinement of an in Situ Conversion Reaction for a Rechargeable Magnesium Ion Battery. *Chem. Commun.* **2018**, *54*, 1714–1717.

(26) Murgia, F.; Stievano, L.; Monconduit, L.; Berthelot, R. Insight into the Electrochemical Behavior of Micrometric Bi and Mg₃Bi₂ as High Performance Negative Electrodes for Mg Batteries. *J. Mater. Chem. A* **2015**, *3*, 16478–16485.

(27) Zhang, Q.; Takeuchi, E. S.; Takeuchi, K. J.; Marschilok, A. C. High Energy Density Electrode Materials for Rechargeable Magnesium Batteries. *ECS Trans.* **2015**, *66*, 171–181.

(28) Limthongkul, P.; Jang, Y.-I.; Dudney, N. J.; Chiang, Y.-M. Electrochemically-Driven Solid-State Amorphization in Lithium-Silicon Alloys and Implications for Lithium Storage. *Acta Mater.* **2003**, *51*, 1103–1113.

- (29) Baggetto, L.; Hah, H.-Y.; Jumas, J.-C.; Johnson, C. E.; Johnson, J. A.; Keum, J. K.; Bridges, C. A.; Veith, G. M. The Reaction Mechanism of SnSb and Sb Thin Film Anodes for Na-Ion Batteries Studied by X-Ray Diffraction, ^{119}Sn and ^{121}Sb Mössbauer Spectroscopies. *J. Power Sources* **2014**, *267*, 329–336.
- (30) Suryanarayana, C. Mechanical Alloying and Milling. *Prog. Mater. Sci.* **2001**, *46*, 1–184.
- (31) Fecht, H. J.; Hellstern, E.; Fu, Z.; Johnson, W. L. Nanocrystalline Metals Prepared by High-Energy Ball Milling. *Metall. Trans. A* **1990**, *21*, 2333.
- (32) Matsui, M.; Arthur, T. S. Active Material for Rechargeable Battery, US Patent 8685564 B2, April 1, 2014.
- (33) Johnson, C. S.; Vaughey, J. T.; Thackeray, M. M.; Sarakonsri, T.; Hackney, S. A.; Fransson, L.; Edström, K.; Thomas, J. O. Electrochemistry and In-Situ X-Ray Diffraction of InSb in Lithium Batteries. *Electrochem. Commun.* **2000**, *2*, 595–600.
- (34) Ersching, K.; Campos, C. E. M.; de Lima, J. C.; Grandi, T. A. Structural and Thermal Studies of Mechanical Alloyed InSb Nanocrystals. *Mater. Chem. Phys.* **2008**, *112*, 745–748.
- (35) Lu, Z.; Schechter, A.; Moshkovich, M.; Aurbach, D. On the Electrochemical Behavior of Magnesium Electrodes in Polar Aprotic Electrolyte Solutions. *J. Electroanal. Chem.* **1999**, *466*, 203–217.
- (36) Martinez-Ripoll, M.; Haase, A.; Brauer, G. The Crystal Structure of $\alpha\text{-Mg}_3\text{Sb}_2$. *Acta Crystallogr. B* **1974**, *30*, 2006–2009.

(37) Wołczyrz, M.; Kubiak, R.; Maciejewski, S. X-ray investigation of thermal expansion and atomic thermal vibrations of tin, indium, and their alloys. *Phys. Status Solidi B* **1981**, *107*, 245–253.

(38) Vaughey, J. .; Johnson, C.; Kropf, A.; Benedek, R.; Thackeray, M.; Tostmann, H.; Sarakonsri, T.; Hackney, S. A.; Fransson, L.; Edström, K.; et al. Structural and Mechanistic Features of Intermetallic Materials for Lithium Batteries. *J. Power Sources* **2001**, *97–98*, 194–197.

(39) Ino, N.; Hirabayashi, M.; Ogawa, S. X-Ray and Thermal Analyses of the Order-Disorder Transition in Magnesium-Indium Alloys. *Trans. Jpn. Inst. Met.* **1965**, *6*, 172–178.

(40) Watson, L. M.; Marshall, C. A. W.; Cardoso, C. P. On the Electronic Structure of the Semiconducting Compounds Mg_3Bi_2 and Mg_3Sb_2 . *J. Phys. F Met. Phys.* **1984**, *14*, 113.

TOC Graphic

